Astron. Astrophys. 332, 111–120 (1998)

ASTRONOMY
AND
ASTROPHYSICS

Radio pulsar microstructure at 1.41 and 4.85 GHz

Ch. Lange, M. Kramer, R. Wielebinski, and A. Jessner

Max-Planck-Institut für Radioastronomie, Auf dem Hügel 69, D-53121 Bonn, Germany

Received 12 June 1997 / Accepted 31 October 1997

Abstract. We report on observations of microstructure at 4.85 and 1.41 GHz of pulsars strong enough for the observation of single pulses with time resolution between 7 μs and 160 μs. All five pulsars observed at 4.85 GHz show microstructure in a large fraction of their pulses. We confirm that microstructure seems to be a common property of the pulsar emission mechanism and not only an additional feature of some pulsars. We show that, for those pulsars observed earlier at lower frequencies, there is little variation in microstructure parameters at different frequencies. The fraction of pulses showing microstructure tends to be higher at 4.85 GHz when compared with lower frequency observations. We argue that the short time-scale of microstructure reflects the extension of the emitting structures.

Key words: methods: statistical – stars: neutron – pulsars individual: PSR B0329+54, PSR B0540+23, PSR B0823+26, PSR B0950+08

1. Introduction

It was already evident from the very first measurements after the discovery of pulsars that their radiation varies significantly from pulse to pulse. Some single pulses show more or less smooth substructure while others have their emission concentrated in short features of typically several hundred microseconds (Craft et al. 1968). These short time-scale features of pulsar radiation, called *microstructure*, have been observed for some pulsars with time-scales down to several microseconds duration (Bartel & Sieber 1978). For the Crab pulsar variations were shown to occur on time-scales down to several nanoseconds (Hankins 1996).

Boriakoff & Ferguson (1981) showed that microstructure is intrinsically broadband. Other investigations found a typical width of micropulses for some pulsars, i.e. PSRs B1133+16 (Hankins 1972) and B0950+08 (Rickett et al. 1975), although pulses with narrower structure than this typical duration were also present. In some single pulses, a periodic behaviour of microstructure was observed (e.g. Ferguson et al. 1976) with periods varying from pulse to pulse (e.g. Figs. 1 & 3). For some pulsars (e.g. PSR B1133+16), there are also indications that periodic microstructure tends to occur more likely at preferential periods (Ferguson & Seiradakis 1978).

Several attempts have been made in the past to explain this kind of emission. One of the most common assumptions is to relate the micropulse emission directly to the emission process (Buschauer & Benford 1980). A different explanation assuming neutron star vibrations to be responsible for periodic microstructure is given by van Horn (1980). Another way to explain narrow periodic structures is to assume a propagation effect, e.g. due to a shearing plasma in the pulsar magnetosphere, as proposed by Harding & Tademaru (1981). Most of the models, however, can be sorted into two groups:

- In the first group of models thin flux tubes along magnetic field lines carry streaming bunches of charged particles radiating in their propagation direction. The width of the microstructure would, according to these models, result from the angular beam width of the radiation. As the pulsar rotates this beam will sweep through the line of sight creating emission with a duration proportional to the beam width (see e.g. Benford 1977).
- The second group of models requires radial structures streaming away from the pulsar along the open field lines, which consist (like in the first group) of charged particles. When they reach a certain height above the pulsar they emit radiation, creating a micropulse with a duration depending on the thickness of the emitting structure (Cordes 1981).

The micropulse time-scale is a parameter which can help to find restrictions for these models. In the framework of the first group of models (hereafter referred to as the beaming-model), the energy of out-streaming charges, i.e. the γ factor of their kinetic energy, is related to the beam width of the radiation emitted by the moving particles. In the second group of models, the micropulse duration gives the real emission time-scale.

In order to estimate the relevance of microstructure for pulsar radiation it is of additional interest to have information on the likelihood of single pulses to contain microstructure. Many pulsar parameters, as for example the total intensity and the shape of the integrated pulse profile, vary with the observing frequency. Due to the steep spectrum of pulsar radiation, former observations of microstructure were mostly taken at frequencies up to approximately 1 GHz. In this paper we investigate the behaviour

Send offprint requests to: C. Lange (clange@mpifr-bonn.mpg.de)

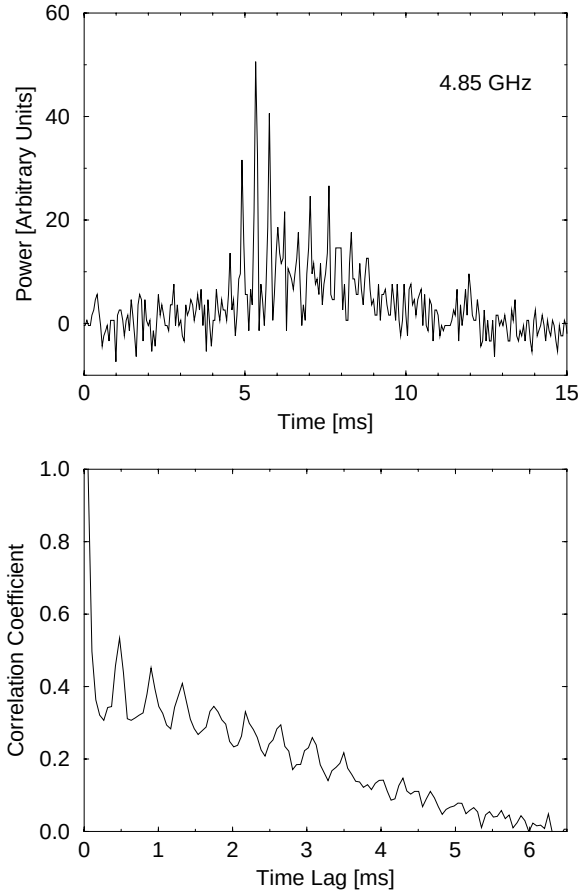

Fig. 1. An example of a single pulse of PSR B0950+08 with periodic microstructure and its ACF at 4.85 GHz. The time resolution is 53 μs.

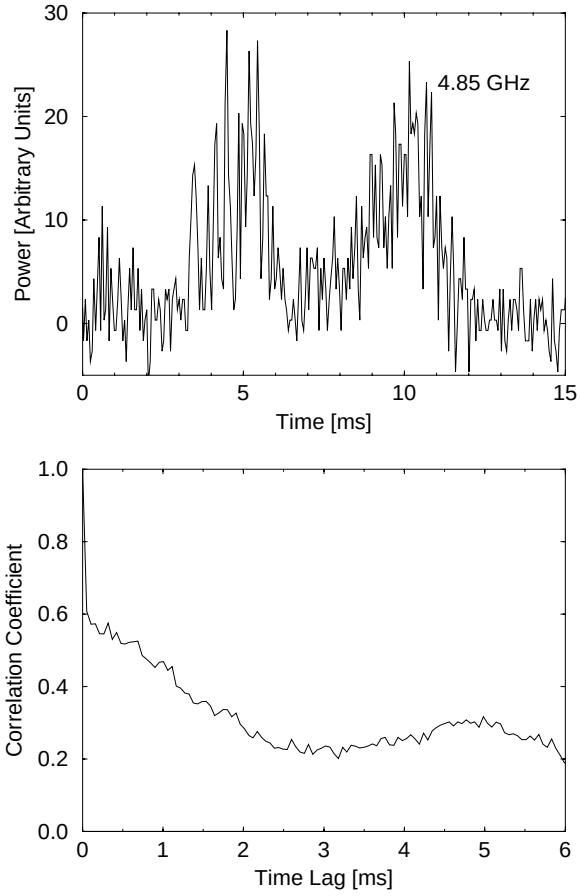

Fig. 2. Single pulse of PSR B0950+08 with non-periodic microstructure and its ACF. The time resolution is 53 μs.

of the microstructure parameters described above at 4.85 GHz and 1.41 GHz respectively.

2. Observations

Our observations were made with the Effelsberg 100-m radio telescope of the Max-Planck-Institut für Radioastronomie. The system temperatures on cold sky of both the 1.41 and 4.85 GHz receivers were about 30 K. A list of pulsars and their observing parameters are given in Table 1. At 1.41 GHz we used an incoherent pulsar de-disperser described by Kramer (1995) for dispersion removal, which provides 60×666.67 kHz channels per polarisation. At 4.85 GHz we detected the full selected bandwidth without de-dispersion. This bandwidth was selected in such a way that the effective time resolution

$$t_{\rm eff} = \sqrt{t_{\rm samp}^2 + t_{\rm DM}^2} \quad (1)$$

with the dispersion smearing $t_{\rm DM}$ was only marginally larger than the sampling time $t_{\rm samp}$. For more details see Table 1 where we also present the used centre frequency and the duration of the individual observation.

At both frequencies left-hand and right-hand circularly polarised signals were detected and digitised by 10-MHz voltage-to-frequency converters. In the off-line reduction both polarisations were added to achieve total power signals.

3. Data analysis

For data analysis we used only single pulses with a signal-to-noise ratio (SNR) of at least 9. These pulses were selected by a routine described by Ferguson & Seiradakis (1978). A constant baseline was subtracted from each selected single pulse.

3.1. Microstructure time-scales

Usually averaged auto-correlation functions (ACFs) of single pulses are studied to determine microstructure time-scales (e.g. Cordes et al. 1990, Kardashev et al. 1978). Here we define the ACF of the ith single pulse, as

$$a_i(n) = K_i \sum_{j=1}^{N_{\rm bin}} I_i(j) \cdot I_i((j+n) - N_{\rm bin} \cdot \Theta(j+n-N_{\rm bin})) \quad (2)$$

where $I_i(j)$ is the intensity in the j^{th} sample of a single pulse in arbitrary units and Θ the Heavyside function. K_i is a nor-

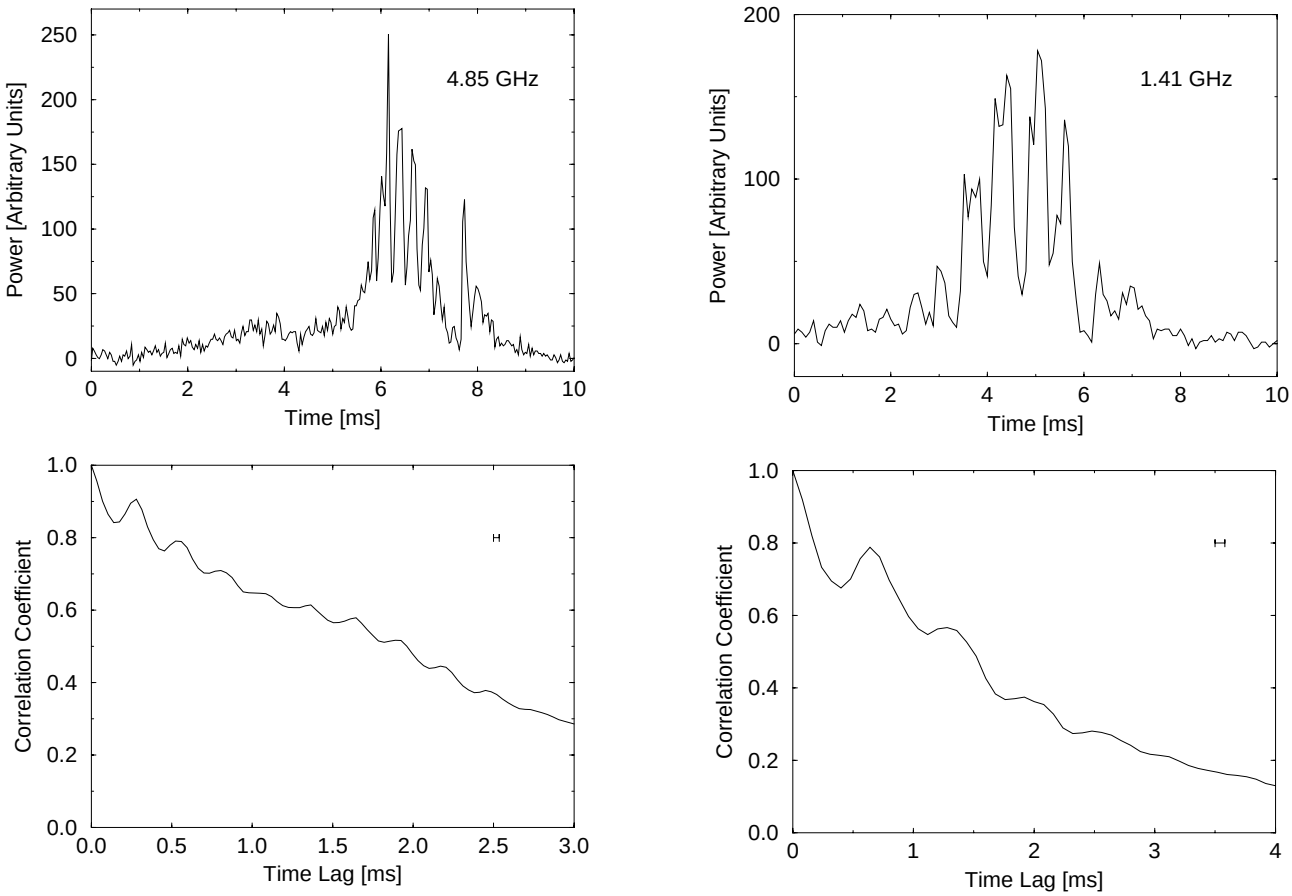

Fig. 3. Two single pulses (above) of PSR B1133+16 and their ACFs (below) at 4.85 GHz (left) and 1.41 GHz (right) with a sampling time of 35 μs and 80 μs respectively, represented by the error bars. Both pulses show quasi-periodic microstructure. The sampling times are too small to place error bars in the single pulse plots.

malisation factor and N_{bin} (=1024) is the number of samples per pulse. The definition of the averaged ACF of a data set of k single pulses is then

$$\langle ACF \rangle(n) = \frac{1}{k} \sum_{i=1}^{k} a_i(n), \tag{3}$$

where the a_i(n) is the single pulse ACF as in Eq. (2).

Hankins (1972) found the averaged ACFs of single pulses of PSR B0950+08 and PSR B1133+16 observed at 111.5 MHz, 196.5 MHz and 318 MHz respectively to be divided into two distinct regions. A long feature extends to the width of the averaged pulse profile, and a shorter one is also present. Hankins defined the point of intersection of two straight lines, fitted to the ACF to represent the two regions, as time-scale of microstructure. Rickett et al. (1975) interpreted this point as the typical time duration of micropulses.

Hankins chose the normalisation constant K_i in Eq. (2) so that the zero-lag in the ACF became unity. In contrast to this we set K_i to unity. The advantage of our ACF definition is, that here the single pulses are given a weight to optimise the SNR in the averaged ACF. On the other hand this bears the disadvantage that the ACF might be dominated by a few strong pulses (see later discussion). In order to reduce the noise, we zeroed the off-pulse regions in the data prior to calculating the ACF. Examples of single pulses and their ACFs for PSRs B0950+08 and B1133+16 observed at 1.41 GHz and 4.85 GHz respectively are given in Figs. 1, 2 and 3.

We formed averaged ACFs of the single pulses for each pulsar selected from our data set. Some of these averaged ACFs show a clear transition between a steep and narrow ACF region and a broad long-time region, similar to the ACFs described by Hankins (see Fig. 4). At this point of transition the ACF becomes significantly flatter, hence we will call it the ACF turn-off point.

Due to the resolution of our data, the part of the ACF representing the narrow region often contains only few data points. In contrast to Hankins' analysis, the long-time ACF regions of our data often show strong systematic deviations from a straight line. A least square fit for two straight lines to our data seems therefore not appropriate. We derived the turn-off points in average ACFs as the intersection of two straight lines, which were determined as tangents to the parts of the ACF at smaller and larger lags. These tangents were found by visually fitting a straight

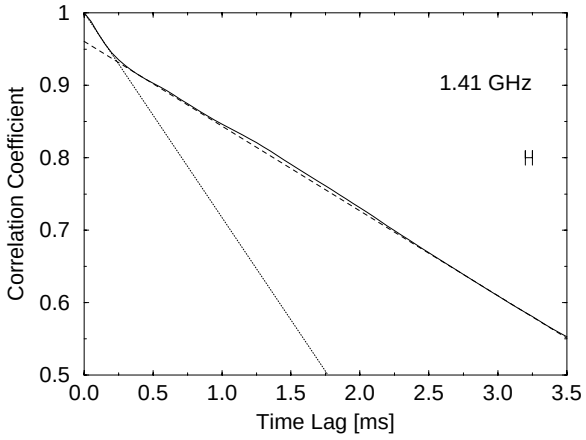

Fig. 4. Tangents to the averaged single pulse ACF of PSR B2016+28 at 1.41 GHz. The averaged ACF is represented by the solid line, the dotted and dashed line show the tangents to the short and longer parts of the ACF respectively. The error bar represents the sampling time of 50 μs.

Table 1. Observational parameters: pulsar name, observing bandwidth, time resolution of the data relating to the sampling time, effective resolution taking the dispersion smearing into account and duration of the scan.

PSR	Freq. [GHz]	BW [MHz]	t_{samp} [μs]	t_{eff} [μs]	Duration [min]
B0329+54	4.85	80	160	223	30
B0540+23	1.41	40	60	156	30
B0823+26	4.85	40	60	83	30
B0950+08	4.85	200	53	68	2×30
B1133+16	1.41	40	80	80	10
	4.85	80	35	45	2×30
	4.85	40	18	23	30
	4.85	20	7	10	30
B1929+10	4.85	200	53	70	30
B2016+28	1.41	40	50	57	10

line which touches the ACF at least twice as a lower bound (see e.g. Fig. 4).

One reason for the deviations of the long-time ACF region from straight lines is the quasi-periodic behaviour of emission maxima in single pulses (e.g. Ferguson & Seiradakis 1978). If strong pulses show periodic behaviour, or a large number of pulses in the data set have similar periodicities, a broad maximum will be generated in the averaged ACF. Such maxima might fall onto the ACF turn-off point. In these cases microstructure time-scales can become invisible in the averaged ACF or a turn-off point may seem to be shifted (see paragraph on PSR B1133+16 in Sect. 4).

For that reason we applied a second data reduction method, searching the position in each of the single pulse ACFs, where they become significantly flatter. A description of this method is given in Appendix 7. Similar to the microstructure time-scale definition by Hankins (1972), we interpret this ACF flattening point as the single pulse time-scale. We compose histograms of such microstructure time-scales in single pulses. Typical micropulse time-scales exhibit themselves as either a clear maximum (Fig. 12) or step-like upper limit (Fig. 10) in these histograms. However, in some cases, when microstructure was apparent in single pulses, the histogram represented a smoothly decaying function, so that typical time-scales could not be found by the second method.

In general, both applied methods yield similar results. The only exception is PSR B1133+16, where the results from both types of analysis disagree significantly. The results from the first method are influenced by quasi- periodic behaviour within the pulses, but our second method is unaffected and therefore more reliable.

A Gaussian approximation:

$$t_{\rm ms} = \sqrt{t_{\rm raw}^2 - t_{\rm eff}^2} \tag{4}$$

was used to correct the time-scales for the broadening of our data due to dispersion and sampling. Here $t_{\rm raw}$ is the measured time-scale, $t_{\rm eff}$ the effective resolution from Eq. (1) and $t_{\rm ms}$ is the intrinsic micropulse width. We expect the sampling time to be the limiting factor for our accuracy.

3.2. Periodicities in microstructure

We analysed the single pulse data in two independent ways to investigate the possible existence of (quasi-) periodicities in the microstructure. The first method uses averaged periodicity properties of single pulse ACFs. By using the un-normalised ACFs, we give each single pulse ACF the weight of the sum of its squared bins in total power. Maxima in the averaged ACF were often superposed by the generally strong decline of the function. For that reason we decided to use ACF derivatives. In terms of Fourier space, we suppressed effects of wider pulse features by weighting with the frequency. Frequencies, typical for microstructure were obtained from the power spectra of these ACF derivatives (in the following abbreviated by ADP):

$$\mathrm{ADP}(I(t)) = |\mathscr{F}(\frac{d}{dt}a(I(t)))|^2 \tag{5}$$

where $I(t)$ is the time dependent intensity and $\mathscr{F}$ the Fourier transform. The average of these ADP was taken over the selected single pulses.

It follows from the auto correlation theorem, that no spurious frequencies are added to the data by this procedure. So maxima observed in the averaged ADP can be identified with periodicities occurring in microstructure. In Fig. 5, we demonstrate the improvement in signal-to-noise ratio by using the ADP compared to the averaged power spectrum.

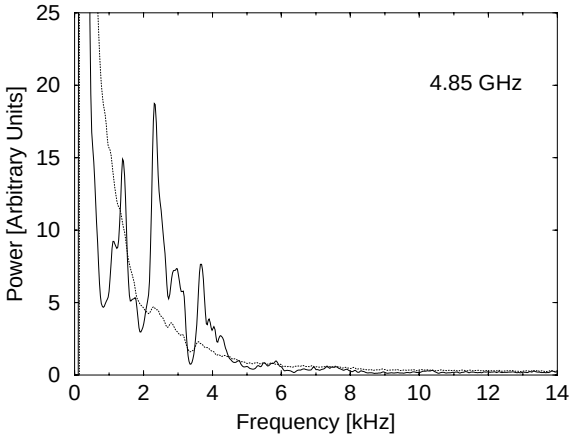

Fig. 5. Comparison between averaged power-spectrum (dotted curve) and ADP (solid line) of PSR B1133+16. The ADP shows strong maxima, only faintly visible in the power-spectrum.

Having no better alternative the large weight given to strong single pulses makes possible, that in a small sample only very few pulses with periodic structure can add strong maxima to the averaged ADP. In order to recognise maxima originating in only a few pulses, we calculated histograms of (quasi-) periods found in single pulses. After identifying the periods from local maxima in the single pulse ADP, a visual inspection of the single pulses and their ACF decided which of the pulses shows periodicities strong enough to be evaluated. As evident from Figs. 1, 2 and 3 the ACF is a helpful tool for the decision if a periodicity is present in single pulse data. This careful inspection was necessary as there are great differences in the microstructure between pulsars and even between individual pulses from the same source (see Cordes et al. 1990).

4. Results

Apart from the detection of microstructure on nanosecond timescales in the giant pulses of the Crab pulsar at 4.885 GHz by Hankins (1996), this work presents the first microstructure detection for pulsars at a frequency as high as 5 GHz. Our observations extend the frequency range of observed microstructure so that it now covers 6 octaves. For PSRs B0540+23, B0823+26 and B1929+10 these are the first microstructure detections ever. We found microstructure in all pulsars observed. This leads to the suggestion that the phenomenon occurs not only for the few strong pulsars which are already known to exhibit microstructure, but it is a common feature for many, if not all pulsars.

In our analysis we find time-scales as either a typical duration or an upper limit for the duration of microstructure. We thus take the number of pulses from the time-scale histogram, which are shorter or equal to the typical time-scale, described in 3.1, as the number of pulses exhibiting microstructure. For those pulsars, where no typical duration was evident, we could clearly distinguish pulses with structure on short time-scales from those with widely spread emission, because the difference between these time-scales is usually more than one order of magnitude. Table 2 gives the fraction of the selected single pulses, which show microstructure. In the following we give a more detailed description of our results for the individual pulsars.

For PSR B0329+54 microstructure is found in approximately 30% of the 769 strong single pulses, selected from about 2500 in the whole scan. Some of them also show a periodic behaviour, with periodicities ranging from 600 to 1500 microseconds. Nevertheless neither a typical microstructure period nor time-scale within the applied time resolution could be obtained. Since the correlation coefficient of the first time lag in the averaged ACF is only by 5% below that at zero-lag, it is not very likely, that there is a significant structure at shorter time-scales unless shorter than our resolution of 160 μs.

About 50% of the 242 single pulses selected from an observation of PSR B0540+23 show microstructure. Most of the micropulses ($\approx$30% of all selected pulses) come on time-scales shorter or equal to 390 $\pm$ 60 μs. Corrected for the time resolution these 390μs correspond to an intrinsic width of 360 μs. Nevertheless no typical width for the micropulses could be obtained from the averaged ACF. In some single pulses the microstructure appears to be periodic, however, we did not find a preferred period for our sample.

As PSR B0823+26 allows observations with better time resolution, the situation is somewhat clearer for this source. Here microstructure is evident in about 30% of the selected pulses. We could not detect a turn-off in the averaged ACF and no preferred micropulse width in the histogram. A pronounced maximum is present in the ADP between 1 kHz and 2 kHz, corresponding to the maximum in the histogram of periodicities between 360 μs and 660 μs (Fig. 6). However, as we found only few pulses showing clear periodicities, the statistics are too poor to draw a conclusion about the existence of a preferred frequency. We also observe microstructure with longer periods. Periods shorter than these were neither seen in the single pulses nor in the averaged ADP, which showed to be especially sensitive for short periodicities. Thus it is rather improbable that this pulsar shows significant structures with frequencies between 2 kHz and 8 kHz (Fig. 7).

The averaged ACF of PSR B0950+08 shows a turn-off-point at time-lag four, which was confirmed by single-pulse statistics. The intersection of the tangents yields a typical width of 185 μs (Fig. 8). Corrected for the sampling rate and dispersion broadening of the micropulses we obtain a value of 170 $\pm$ 53 μs. Approximately 70% of the 344 pulses selected show microstructure. We separately determined the frequency of occurrence of microstructure in 51 pulses with SNR of at least 18. We found microstructure in 35 of them, which appears to be a similar fraction. This may indicate that the relevance of microstructure is the same for those pulses, which are too weak to be analysed. Although we could clearly observe periodic microstructure in some (i.e. 42) of the single pulses, no preferred frequency could be found in the ADP.

For PSR B1133+16 we could not only determine the fraction of single pulses showing microstructure but also a time-scale and range of microstructure periods. Two data sets of 35 μs

Table 2. Microstructure parameters derived at 4.85 GHz and 1.41 GHz respectively. The table gives source name, observing frequency, pulse period, fraction of selected pulses with microstructure, typical pulse widths and ranges of preferred microstructure periods. The last four columns give micropulse widths and periods related to the pulse period and multiplied with velocity of light.

PSR	Freq. [GHz]	PSR-Period [s]	Fraction [%]	t_{ms} [μs]	MS-Period [μs]	$\frac{t_{ms}}{P}$ [10^{-4}]	$\frac{\text{MS-Period}}{\text{PSR-Period}}$ [10^{-4}]	$t_{ms}\cdot c$ [km]	MS-Period $\cdot c$ [km]
B0329+54	4.85	0.715	30	$<$1500	600 – 1500	$<$21	8 – 21	$<$500	180 – 450
B0540+23	1.41	0.246	50	$<$360	—	$<$15	—	$<$108	—
B0823+26	4.85	0.531	30	—	360 – 660	—	6.8 – 12.5	—	108 – 180
B0950+08	4.85	0.253	70	170	—	6.7	—	51	—
B1133+16	4.85	1.188	50	365	$\leq$800	3.1	$\leq$6.7	110	$\leq$240
B1929+10	4.85	0.227	50	—	—	—	—	—	—
B2016+28	1.41	0.558	50	230	$\approx$ 640	4.1	$\approx$11.5	69	$\approx$190

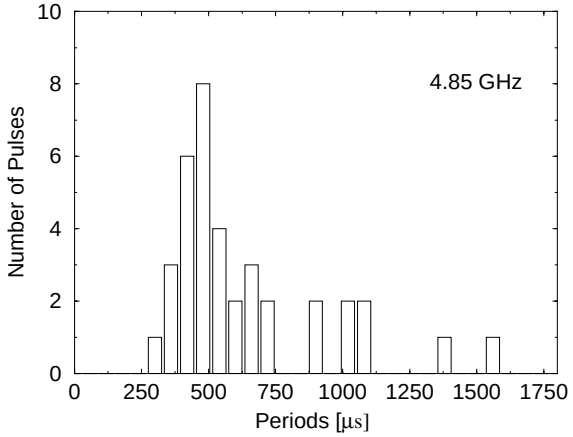

Fig. 6. Typical micropulse periods of PSR B0823+26

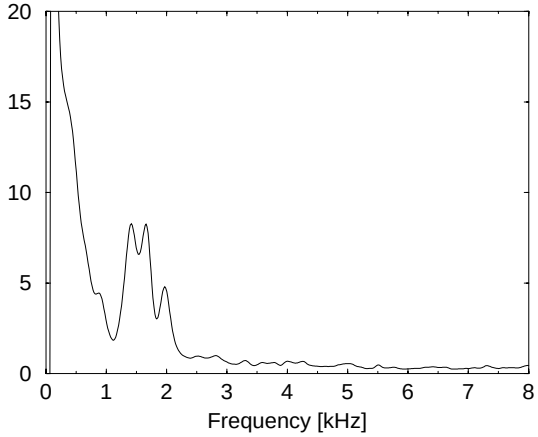

Fig. 7. Averaged ADP of PSR B0823+26

time resolution provided 366 pulses with SNR better than 9σ. About 50% of these include microstructure. From the averaged ACF we derived a typical micropulse width of 150 μs (Fig. 9). This is however not visible in the histogram of the single-pulse micropulse width (Fig. 10), where micropulse widths are common up to about 370 μs. We assume that this upper limit for the microstructure time-scale corresponds to those from former investigations of this pulsar (see Table 3). There is evidence from the ADP of PSR B1133+16, that this pulsar shows periods close to 390 μs (Fig. 11), the width expected from the histogram. We thus derive a typical micropulse width of 365 ± 35 μs. We note that ADPs obtained from different observations with different time resolutions show essentially the same shape. A striking feature is the coincidence of maxima close to 1200 Hz, 2500 Hz and 3750 Hz, strongly suggesting that these frequencies are typical for the microstructure of this pulsar. This frequency range is verified by the histogram of single pulse periodicities.

From 234 single pulses, selected with an SNR of at least 9σ out of 8000 pulses of PSR B1929+10, significantly more than 50% contain microstructure features. The averaged ACF does not show any turn-off point above 150 μs. Nevertheless, a large amount of single pulses show structure on scales around 150 μs. Quasi periodicities between 240 μs and 1 ms are found in 32 single pulses, but we did not find a preferred period in the data.

PSR B2016+28 was observed at 1.41 GHz. Our selection criterion for this pulsar was a single pulse SNR of at least 12. We found microstructure in about 50% of 344 selected pulses. A typical pulse width of 230 ± 50 μs was derived from the tangents fitted to the ACF, in coincidence with the results obtained from the histogram of single pulses (Fig. 12 & 4). We also found periodicities around 640 μs.

5. Frequency behaviour of pulsar parameters

The main aim of our observations was to assess the importance of microstructure for the radio emission process in pulsars. We were particularly interested in the frequency dependence of the relevant parameters of this phenomenon and therefore made first time microstructure observations for five sources at 4.85 GHz. In this section we will compare our results obtained at 1.4 GHz and 4.85 GHz to those previously derived by other authors.

For many pulsars exhibiting microstructure, a typical width of micropulses could be determined, usually by investigating the turn-off point in the mean single pulse ACF (e.g. Ferguson & Seiradakis 1978). Periodicities were found in pulses of

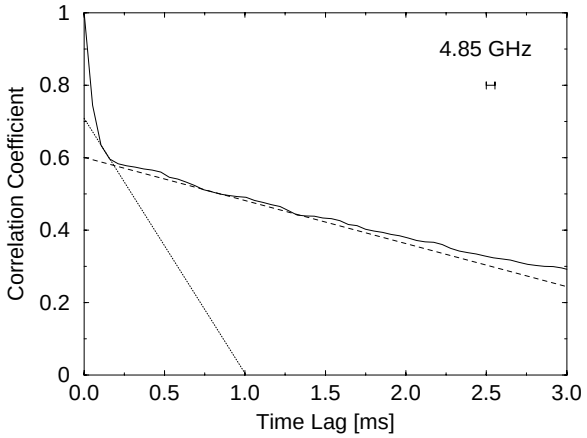

Fig. 8. Averaged un-normalised ACF of PSR B0950+08 (solid line). The dotted and dashed line represent tangents fitted visually to the short and long ACF structures respectively. The error bar represents the sampling time of 53 μs.

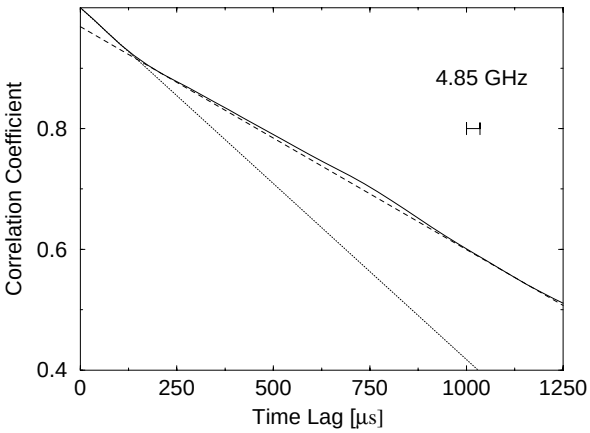

Fig. 9. Averaged un-normalised ACF of PSR B1133+16. Tangents are fitted to the short scale (dotted line) and wider (dashed line) parts of the ACF. The error bar represents the sampling time of 35 μs.

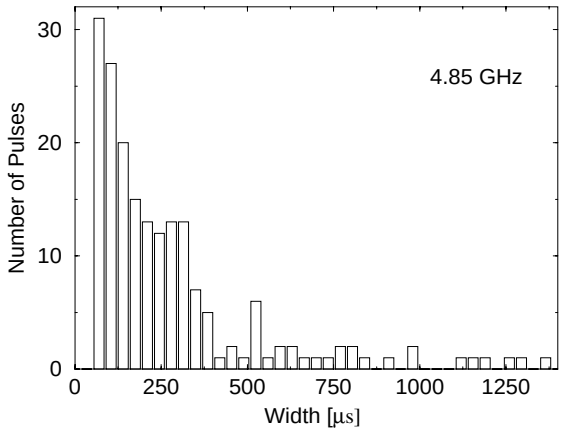

Fig. 10. Time-Scales of PSR B1133+16 microstructure

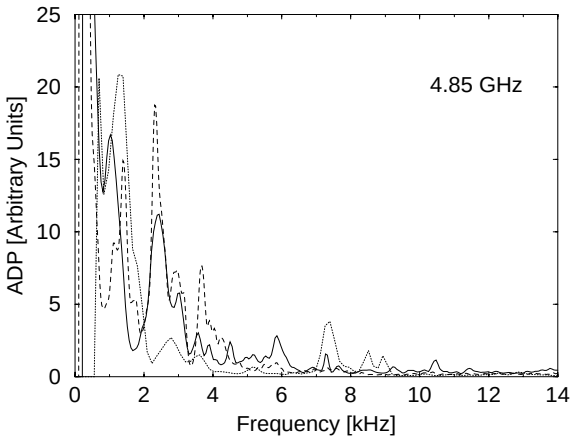

Fig. 11. Averaged ADP of PSR B1133+16 with time resolution of 35 μs (dashed line), 18 μs (solid line) and 7 μs (dotted line) respectively. The digitalisation in the high time-resolution data ADP is an effect of the discrete Fourier transform.

PSRs B0329+54 (Kardashev et al. 1978), B0950+08 (Hankins & Boriakoff 1978), B1133+16 (Ferguson & Seiradakis 1978) and B2016+28 (Cordes 1976, Cordes et al. 1990, Boriakoff 1976). A summary of typical micropulse widths and quasi periodicities found at lower frequencies for these pulsars is presented in Table 3. For PSR B0950+08, Popov et al. (1987) found microstructure in 20% and 50% of the single pulses observed, at 69.8 MHz and 102.5 MHz respectively. Boriakoff & Ferguson (1981) observed a 66% correlation of PSR B0950+08s microstructure between 430 and 1406 MHz. Simultaneous multi-frequency observations are crucial to resolve this issue, and are planned in the future. Such observations can be done with the facilities of the European Pulsar Network.

Most of the publications do not provide information on the errors for the derived parameters. The typical micropulse width of PSR B1133+16 at 111.5 MHz and of PSR B0950+08 at 430 MHz given in Table 3 vary in different publications. This is probably more due to the criterion of pulse selection than to systematic errors in data analysis (Ferguson & Seiradakis 1978). Despite this uncertainty such typical widths, which are a characteristic feature of microstructure, are only weakly dependent on frequency if at all. These results indicate not only the appearance of microstructure but also its time-scales show a broad band behaviour.

It has been questioned in the past, whether there exist preferred periodicities in the microstructure of PSR B1133+16. Ferguson & Seiradakis (1978) found harmonically related clumps in their histogram of quasi-periodicities of this pulsar. Cordes et al. (1990) contested this view as resulting evidently from their small number of points. Fig. 11 shows coinciding maxima of data scans with different resolution for averaged ADPs of PSR B1133+16. The similarity between the maxima in these ADPs supports the conjecture of preferred periodicities in the microstructure of this pulsar.

The maxima show the relation 1 : 2 : 3, so that a harmonic relationship is plausible. The fundamental frequency would then

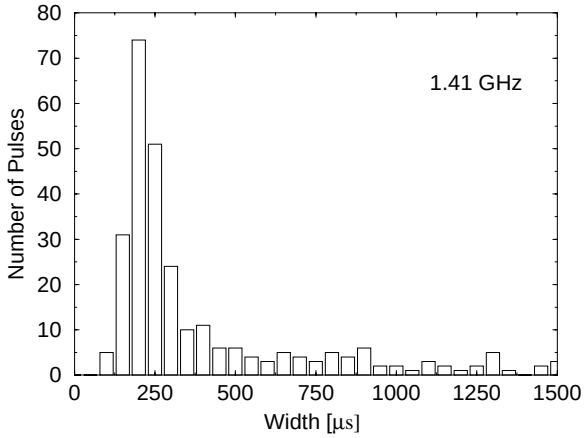

Fig. 12. Time-Scales of PSR B2016+28 microstructure

Table 3. Typical microstructure widths and periods from the literature.

PSR	Freq. [MHz]	t_{ms} [μs]	MS-Period [μs]	Ref.
B0329+54	102.5	—	340	KAR78
B0950+08	111-318	200	—	RIK75
	430	170	—	COR77
	430	130	400–600	HAN78
B1133+16	81.3–102.5	500	—	POP87
	111.5	574	—	HAN72
	111.5	429	150	FER76
	196	651	—	HAN72
	318	525	—	HAN72
	430	340	—	COR77
	1720	380	180–720	FER78
	2650	420	180–720	FER78
B2016+28	430	280	600–1100	COR76
	430	—	900	BOR76
	606	—	500–750	COR76

be approximately 1250 Hz, corresponding to a period of 800 μs with harmonics at 400 μs and 270 μs. These periods, which we found at 4.85 GHz, are similar to those from Ferguson & Seiradakis (1978) at lower observing frequencies. The value of 800 μs for the fundamental period comes close to twice the upper limit of micropulse widths for this pulsar.

6. Discussion

For all observed pulsars, a large fraction of the single pulses (varying between 30% and 70%) show microstructure. This result, combined with the fact that the structure is observed to appear over the whole frequency range where strong single pulses can be seen, supports the idea that microstructure is an important feature of pulsar radiation. It appears more likely that microstructure is closely connected to the emission process, rather than the product of a process occurring in different parts of the pulsar magnetosphere (Ferguson & Seiradakis 1978).

Table 4. Micropulse widths and lower limits for the γ-factors of out-streaming particles according to the beaming interpretation. In column 4 an orthogonal rotator is assumed, while column 5 and 6 are derived for geometries given by Lyne & Manchester (1988) and Rankin (1993), respectively

PSR	P [s]	t_{ms} [μs]	$\gamma_{\alpha=90}$	γ_{LM}	γ_R
B0950+08	0.253	170±25	240	2300	1150
B1133+16	1.188	365±35	520	670	720
B2016+28	0.558	240±50	390	610	620

A point source moving with relativistic energies will have its radiation beamed towards the direction of motion. If we assume microstructure to be the result of a flux tube of such point sources sweeping through the line of sight, we can derive a lower limit for the particle energy from the micropulse width, assuming infinitely narrow flux tubes:

$$\gamma = \frac{1}{\phi \cdot \sin\alpha} = \frac{P}{2\pi t_{\rm ms} \cdot \sin\alpha}. \quad (6)$$

Here ϕ is the micropulse width in radians compared to the pulse period, α the angle between the line of sight and the pulsar rotation axis, P the pulsar period, t_{ms} the micropulse width and γ is the energy of the particles in terms of their rest energy. This interpretation of the beam width is valid for all mechanisms which assume the emission of radiation by relativistic charged particles accelerated along the curved field lines.

Values for γ, derived by this interpretation are given in Table 4. These are lower limits as we assumed sin α to be unity in our calculations. However, we can also apply viewing geometries as for instance given by Lyne & Manchester (1988) and Rankin (1993), resulting in values presented in columns 5 and 6. Furthermore, micropulses are sometimes narrower than the typical time-scales mentioned. These micropulses would then require even higher particle energies and thus larger γ-factors of microstructure emitting features.

Since we have shown that microstructure is a major constituent of pulsar radiation, we expect the γ-factor of microstructure emitting particles to be similar to the γ for averaged pulsar emission. Our derived lower limits for γ, according to the beaming-model, range from 240 to 520. However, many authors present reasons why γ should not significantly exceed a value of 100 (e.g. Dougherty & Harding, 1982, Asseo, 1993). Although it is difficult to estimate an uncertainty for theoretically derived γ-factors, this discrepancy indicates that an assumption of a beaming model with low Lorentz factors is not supported by our observations.

Assuming lower γ-factors the second interpretation of micropulse widths is more likely. Here, the micropulse width corresponds to the extension of radial structures, streaming out-

wards the pulsar magnetosphere with almost the velocity of light. The thickness of the out-streaming features defined by the time-scales of microstructures would be approximately 51 km, 72 km and 110 km for PSR B0950+08, PSR B2016+28 and PSR B1133+16, respectively. For all these pulsars they are of the same order of magnitude as the emission height of the radiation (von Hoensbroech & Xilouris 1997). This relation was already proposed by Hankins (1972), to explain the similarity of the microstructure time-scales of PSR B1133+16 between 111.5 MHz and 318 MHz. Our high frequency results gives further support for this model.

7. Conclusions

The microstructure of the investigated pulsars is found to be present in a large fraction of the strong single pulses at a frequency as high as 5 GHz. This fraction varies between 30 % and 70 %, depending on source. For the pulsars we observed, where also low frequency results are available, we do not see a significant difference between microstructure properties at high or low frequencies. Microstructure of PSR B0950+08 tends to be more common at 5 GHz than at lower frequencies. This may indeed indicate that microstructure is an intrinsic property of the initial particle beam.

We have given arguments that assuming microstructure time-scales to arise from the beaming width of emitting flux tubes, implies fairy high lower limits to the γ-factors of micropulse emission. Since we found that a high fraction of pulses show short time-scale emission, we expect these γ-factors to be close to the average for the pulsar emission. If the averaged γ is significantly lower, as expected by a number of theories for the emission process, we would therefore favour a second interpretation of the microstructure time-scales. According to this the micropulse duration is generated by the dimension of the emitting structure.

Hankins (1972) found the similarity of the time-scales over the frequency range between 111.5 and 318 MHz an indication that they represent the scale size of the emitting region. We found this similarity even at 4.85 GHz. The thickness of microstructure emitting features is moreover comparable to the emission heights in the literature.

Acknowledgements. We want to thank R.T. Gangadhara, Alexis von Hoensbroech, Simon Johnston, Duncan Lorimer, Peter Müller and Wolfgang Sieber for helpful discussions and advice.

Appendix A: micropulse widths in single pulses

One part of our investigations was the determination of typical widths of structures in single pulses. The ACF is a helpful tool for analysis of single pulses. Narrow structures in the pulse contribute only to the ACF up to a scale corresponding to their width. So if there is structure on narrow time-scales in a single pulse, the ACF becomes flatter from that point where those narrow features no longer contribute to it.

Thus for finding typical time-scales of the features of single pulses we look for such flattening in single pulse ACFs. We created an algorithm, named TOP (Turn-Off Point), to calculate typical time-scales from single pulses. The routine searches for strong ACF flattening. To avoid misidentification due to noise in the ACF, the routine checks for this by testing, if the flattening extends over a wider range of ACF points.

The zero-lag ACF point contains the system noise. The first lag can still be influenced by intrinsically very narrow pulse features, broadened by dispersion smearing, even if this effect is smaller than the resolution. TOP starts with the second ACF lag, finishing with a high lag, to process the ACF as follows:

1. For each point n_0 we calculate the local difference $d_0 = A(n_0) - A(n_0 - 1)$, where $A(n)$ is the the n bin ACF-lag. In the same way we compute the next four differences $d_{1\ldots4}$. We aim to find a point, where the ACF becomes significantly flatter. Thus we search an ACF-lag $n_{1\ldots4}$, where the absolute values for the difference $d_{1\ldots4}$ are clearly lower than the absolute value of d_0. For the first $n_{1\ldots4} = n_0 + 1 \ldots 4$, for that $d_{1\ldots4} > d_0/2$ (note that d is usually negative), we take $n_{1\ldots4} - 1$ as candidate point for ACF-flattening. If none of the $n_{1\ldots4}$ fulfils this inequality, procedure 1., described above, is restarted with the next higher bin as a starting point n_0.
2. If an ACF-lag passes the first condition, a second test for non-local flattenings of the ACF is applied. This is useful for the rejection of points due to noise in the ACF. The procedure is to compute the average over the four differences before and after the investigated candidate point

$$A(n_0) - (A(n_0 - 4) < 1.5(A(n_0 + 4) - A(n_0))|\forall n_0 \leq 4 \quad (1)$$

For points near the origin, fewer differences are compared. Failing the criterion (1) leads to the rejection of the candidate point and the algorithm repeats at 1.

The method was tested by comparing its results with those from visual inspection of several hundred single pulses from PSRs B0329+54, B0950+08 and B1133+16 and their ACFs. These test pulses show a great deal of scatter in their widths and appearance. The factors of 2 and 1.5 in TOP for the ACF flattening on short and longer scales respectively were derived to optimise the routine to give the same microstructure widths as seen by visually inspecting the single pulses and their ACFs. They were actually found to coincide in 95 % of the cases for the test data sets. The results were also found to depend only weakly on these factors allowing a variation of up to 10 %.

In addition for most of the pulsars, histograms of single-pulse time-scales that were derived using the algorithm show time-scales coinciding to the pulsars averaged ACF. For these reasons we are confident that the method is reliable and accurate down to one bin, which we also expect to be a realistic value for the accuracy of our visual test. Hence the method enables us to analyse our data up to its natural limits.

References

Asseo E., 1993, MNRAS 264, 940
Bartel N., Sieber W., 1978, A&A 62, 393
Benford G., 1977, MNRAS 179, 311
Boriakoff V., 1976, ApJ 208, L43 (BOR76)

Boriakoff V., Ferguson D. C., 1981, in Proc. of IAU Symposium nr.95: Pulsars, eds. R. Wielebinski, W. Sieber, pp 191
Buschauer R., Benford G., 1980, MNRAS 190, 945
Cordes J. M., 1976, ApJ 208.2, 944 (COR76)
Cordes J. M., 1981, in Proc. of IAU Symposium nr.95: Pulsars, eds. R. Wielebinski, W. Sieber, pp 115
Cordes J. M., Hankins T. H., 1977, ApJ 218, 484 (COR77)
Cordes J. M., Weisberg J.M., Hankins T.H., 1990, AJ 100.2, 1882
Craft H. D., Comella J. M., Drake F. D., 1968, Nat 218, 1122
Dougherty J. H., Harding A. K., 1982, ApJ 252, 337
Ferguson D. C., Seiradakis J. H., 1978, A&A 64, 27 (FER78)
Ferguson D. C., Graham D. A., Jones B. B., Seiradakis J. H., Wielebinski R., 1976, Nat 260, 25 (FER76)
Hankins T. H., 1972, ApJ 177, L11 (HAN72)
Hankins T. H., 1996, in Proc. of IAU Colloq. nr.160, Pulsars: Problems and Progress, eds. S. Johnston, M.A. Walker, M. Bailes, pp 197
Hankins T. H., Boriakoff V, 1978, Nat 276, 45 (HAN78)
Harding A. K., Tademaru E., 1981, ApJ 243, 597
von Hoensbroech A., Xilouris K. M., 1997, A&A 324, 981
van Horn J. H., 1980, ApJ 236, 899
Kardashev N. S., Kuzmin A. D., Nikolaev N. Ya, et al., 1978, Sov. Astron. 22, 583 (KAR78)
Kramer M., 1995, Ph.D. thesis, Universität Bonn
Lyne A. G., Manchester R. N., MNRAS 1988, 234, 477
Popov M. V., Smirnova T. V., Soglasnov V. A., 1987, Sov. Astron. 31, 529 (POP87)
Rankin J. M., 1993, ApJS 85, 145
Rickett B. J., Hankins T. H., Cordes J. M., 1975, ApJ 201, 425 (RIK75)

This article was processed by the author using Springer-Verlag LaTeX A&A style file *L-AA* version 3.